Paramagnetic scattering from metallic Ni

O. Steinsvoll,* C. F. Majkrzak, G. Shirane, and J. Wicksted
Brookhaven National Laboratory, Upton, New York, 11973
(Received 17 October 1983; revised manuscript received 20 April 1984)

We have succeeded in establishing a reliable scattering function $S(Q,\omega)$ for paramagnetic nickel in the range up to $\Delta E=50$ meV, $q=0.4$ Å^{-1}, and $T=1.24T_C$. These studies were performed mainly with unpolarized neutrons, but the polarization analysis was also utilized to completely separate the magnetic cross section. We show that the main part of the magnetic scattering has the form of a broad Lorentzian centered at zero energy transfer. In constant-Q scans, no intensity enhancement was observed at the expected persistent spin-wave position reported by Lynn and Mook. Although constant-E scans show well-defined peaks in agreement with the results of Lynn and Mook, these scans do not signify the existence of persistent spin waves above T_C. The magnetic intensities have been put on an absolute scale by comparing with known phonon and magnon cross sections. In this way, we have derived the paramagnetic response $M^2(Q)$ which is Lorentzian in $\vec{q}$ $(=\vec{Q}-\vec{\tau})$ with correlation lengths that, unexpectedly, correspond to extrapolated values found in the critical region.

I. INTRODUCTION

The magnetism in $3d$ metallic ferromagnets above the Curie temperature has recently been the center of considerable controversy and extensive research. Early neutron scattering experiments performed on nickel by Minkiewicz *et al.*[1] studied the renormalization of spin waves at small q values as the Curie temperature was approached from below. This renormalization indicates that D is scaling as the magnetization as expected from scaling laws. Just below T_C the spin waves become overdamped and there is a continuous transition to critical scattering at and above T_C. However, constant-energy measurements conducted by Mook *et al.* and by Lynn and Mook[2,3] have shown that there remains a ridge of intensity at energy transfers up to 90 meV which develops above T_C from the high-energy spin-wave ridge below T_C. They concluded that this intensity ridge was in fact a propagating spin wave for energy transfers greater than 35 meV. Persistent spin waves have also been reported in metallic iron by Lynn.[4] These experiments have motivated the development of local band theories[5] which assume the existence of short-range order in the paramagnetic phase of ferromagnetic $3d$ metals.

Recently, a series of neutron scattering experiments[6,7] on Ni and Fe as well as compounds in the paramagnetic state have been reported. They have utilized polarization analysis with different polarization alignment relative to the scattering vector to separate the magnetic scattering above T_C from other scattering contributions, such as phonon and nuclear incoherent scattering. In these experiments Brown *et al.*[6,7] have utilized, intentionally, a very broad energy resolution [$\sim$43 meV full width at half maximum (FWHM)] in order to integrate the scattering function $S(Q,\omega)$ over energy to obtain a proper value of $S(Q)$. The results of the experiments of Brown *et al.*[7] on Fe have been interpreted as showing a considerable short-range order which persists well above T_C.[7] Recently, however, Edwards[8] has reinterpreted the Fe results as demonstrating a much smaller value of short-range order. Edward's conclusion was based on the assumption that up to 70% of the magnetic scattered intensity was missing in the data of Brown *et al.*[7] for large-q values. Due to their poor resolution, Brown *et al.*[6,7] could not separate a possible inelastic spin-wave part from magnetic quasielastic scattering. It is, therefore, essential to properly characterize $S(Q,\omega)$ for the $3d$ metals in order to determine how much the spin waves contribute to the magnetic fluctuation scattering above T_C in addition to resolving the size of the short-range order.

This paper contains the results of an investigation using both unpolarized and polarized neutrons with energy resolution sufficient to characterize the magnetic scattering above T_C for metallic nickel. A part of this work has previously been reported.[9] We present constant-intensity contour maps of the scattering function $S(Q,\omega)$ which, quite surprisingly, have the form of the double Lorentzian in q and energy normally found in the critical scattering region. The persistent spin waves obtained from constant-energy scans at temperatures above T_C can now be seen to be a manifestation of this double Lorentzian form of the magnetic scattering intensity.

Using calculated scattering cross sections and integrated intensities of acoustic phonons and magnons we have further been able to normalize our spectrometer in absolute units (b/atom). This scale has been used to convert the integrated magnetic diffuse scattering into the equivalent of effective magnetic moments thereby facilitating the comparison with static susceptibility measurements and previous critical scattering experiments on Ni.[1] Our measurements actually overlap the latter experiments which were performed at small values of q. For larger values of q and energy our measurements extend into the region of (q,ω) space where a so-called persistent spin-wave mode has been observed above T_C.[3]

II. EXPERIMENTAL

The experiments were performed on the same cylindrical single crystal of ^{60}Ni as was used by Minkiewicz *et al.*,[1] with a volume of 2.9 cm^3. Using this particular even-numbered isotope, the nuclear-spin and isotopic incoherent scattering is eliminated and the phonon scattering is reduced by an order of magnitude relative to natural nickel due to the small nuclear coherent scattering amplitude of ^{60}Ni. The [0$\bar{1}$1] axis was almost along the cylinder axis and was chosen to be perpendicular to the scattering plane. The data were collected in the vicinity of the (1,1,1) reciprocal-lattice point by triple-axis scans in the creation mode in the [111] direction. The reciprocal-lattice spacing at T_C is 3.09 Å^{-1}.

In the unpolarized neutron experiments pyrolytic graphite crystals were used as monochromator and analyzer with fixed final energies (E_F) at 14.7, 30.5, and 60 meV. For 14.7 and 30.5 meV, a pyrolytic graphite filter was used in front of the counter. All horizontal Soller collimators were 20′, thus giving energy resolutions (FWHM) at zero energy transfer of about 0.5, 1.4, and 4 meV, respectively. The corresponding q resolutions are 0.012, 0.026, and 0.33 Å^{-1}. The vertical collimation was more relaxed. The higher resolution was used to investigate the linewidth at T_C while the lower resolutions were used when mapping out the more detailed appearance of $S(Q,\omega)$.

In the polarized neutron case we used vertically magnetized composite Heusler alloy monochromators and analyzers with magnetic guide fields and a flat coil spin flipper in the beam path. The focusing analyzer was fixed at 30.5 meV and all collimators were 40′ thus giving an energy resolution of 3.0 meV and a q resolution of 0.054 Å^{-1} at zero energy transfer. The guide field at the sample was produced by a permanent magnetic creating a field of 120 Oe along the scattering vector in the horizontal plane. The flipping ratio was 18 and there was no measurable depolarization of the beam through the sample above T_C.

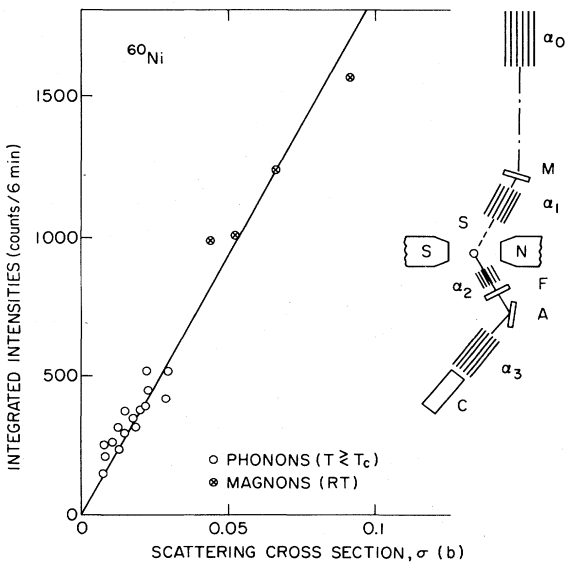

FIG. 1. On the left-hand side we show the calibration curve of our spectrometer for unpolarized neutron scattering from metallic nickel. On the right we show a schematic diagram of our triple-axis spectrometer in the polarized neutron mode. All collimators ($\alpha_1\alpha_2\alpha_3\alpha_4$) were 40′.

The crystal was heated in a vacuum furnace which consisted of hollow copper spherical caps, with heater wires on the outside, joined to a thin equatorial section made from aluminum. Two cylindrical thermal shields were inserted between the heating caps and the outer vacuum jacket. The heating wires were arranged so that the magnetic fields due to the heater currents were compensated in order to eliminate stray fields which could depolarize the beam. A Chromel-Alumel thermocouple was embedded in the crystal for temperature determination. The furnace temperature was kept stable to 0.5 K. The inset in Fig. 1 is a schematical drawing of the spectrometer and its collimation.

The temperature of the sample was calibrated by utilizing the known value of the Curie temperature ($T_C \approx 631$ K). With the spectrometer set at zero energy transfer the intensity of the critical diffuse magnetic scattering was observed by scanning over small q values at a series of temperatures above and below T_C. For each q value the intensity would show a maximum at a certain temperature $T_{\max}(q)$. The values of $T_{\max}$ were then extrapolated to $q=0$ to give T_C. The value of T_C was checked by polarized neutrons by observing the onset of depolarization of the beam through the sample by lowering the temperature through the Curie point. The transition was very sharp and the Curie temperature could be determined to within a fraction of a degree. Polarized and unpolarized measurements gave consistent results.

A technique has been developed which allows both the scattering function $S(Q,\omega)$ and the paramagnetic response $M^2(Q)$ to be put onto an absolute intensity scale. This scale results from theoretically calculated and experimentally measured phonon and magnon cross sections. A full description of this procedure is given in the Appendix.

III. MAGNETIC SCATTERING BELOW AND ABOVE T_C

The form of the scattering function in the critical region is a double Lorentzian in q and ω given by[10]

$$S(Q,\omega)=\frac{2}{3\pi}\frac{S(S+1)}{r_1^2}\frac{1}{\kappa_1^2+q^2}\frac{\Gamma}{\Gamma^2+\omega^2}, \tag{1}$$

where Γ is the half width and κ_1 and r_1 represent the range and strength of the spin correlations, respectively. These parameters are related to the static susceptibility $\chi_\alpha(0)$ by the expression

$$\frac{1}{(r_1\kappa_1)^2}=\frac{\chi_\alpha(0)}{\chi_0},$$

where χ_0 is the value which the static susceptibility has at temperature T when there is no exchange interaction between spins.

Using the triple-axis neutron scattering technique, a series of constant-energy and constant-Q scans in the

[111] direction were performed on ^{60}Ni both below and above T_C. The results of these experiments, which utilized both unpolarized and polarized neutrons, will now be given. A comparison of these results with Eq. (1) will be made in Sec. IV.

Figure 2 shows plots of maximum intensity positions obtained from constant-energy scans performed by us at room temperature, at T_C-58 K and at T_C+100 K. Included in this figure are the spin-wave dispersion relations for similar temperatures obtained via constant-energy scans by Lynn and Mook.[3] The agreement between these dispersion curves and our measurements is quite good. An example of constant-energy scans (labeled "A scans" in Fig. 2) obtained by us using unpolarized neutrons is given in Fig. 3. The energy transfer is 20 meV with scans performed at T_C-58 and T_C+100 K. The LA-phonon peaks have been deleted from this figure.

Constant-Q scans (labeled "B scans" in Fig. 2) were also obtained via unpolarized neutrons. In Fig. 4 we have plotted two typical scans at (1.08,1.08,1.08) for temperatures below and above T_C. The approximate distribution of the magnetic scattering has been drawn with solid lines in these plots. Superimposed on the magnetic ridges is a temperature-independent background scattering centered at zero energy transfer. At high energy the LA-phonon peak is observed while at slightly lower energy some scattering intensity due to interference with the TA-phonon branch is evident.[11] Below T_C a wide spin-wave resonance is observed. The large width of this peak results from the very steep slope of the spin-wave dispersion curve. The combined effects of the resolution function, Bose occupation number, and the steep slope of the spin-wave dispersion curve, leads to a shift to lower energy of the peak position relative to the position expected from the dispersion curve in Fig. 2. Above T_C, the magnetic scattering takes the form of a broad Lorentzian distribution centered at zero energy transfer. The full width of this scattering is considerably larger than the energy resolution indicating that this magnetic scattering is clearly inelastic. Solid lines in Fig. 4 are calculated cross sections convoluted with resolution parameters shown in Table I. The curve for the scan at T_C+100 K is calculated with $\Gamma=9.9$ meV and $\kappa_1=0.19$ Å^{-1} and this spin-wave intensity at T_C-58 K was calculated with $D=233$ meV Å^2 ($\Gamma=\Lambda q^2$). Overall agreement is satisfactory. Figure 5 shows a constant-Q scan using polarized neutrons and spin-flip polarization analysis at T_C+100 K. Using this technique, the phonon disturbance is completely filtered out and the Lorentzian line shape of the magnetic scattering is even more evident.

On the basis of the constant-Q scans with moderate energy resolution ($E_F=30.5$ meV) we have drawn constant intensity contours for the low-energy region of (q,ω) space, close to the (1,1,1) reciprocal-lattice point. The higher-energy region was surveyed by constant-energy scans with $E_F=60$ meV. In Fig. 6 we show a contour map combining the two sets of measurements performed at $T=T_C+100$. The dispersion curve for the persistent spin-wave mode as obtained by Lynn and Mook[3] has been drawn for comparison. The crosses show the positions of

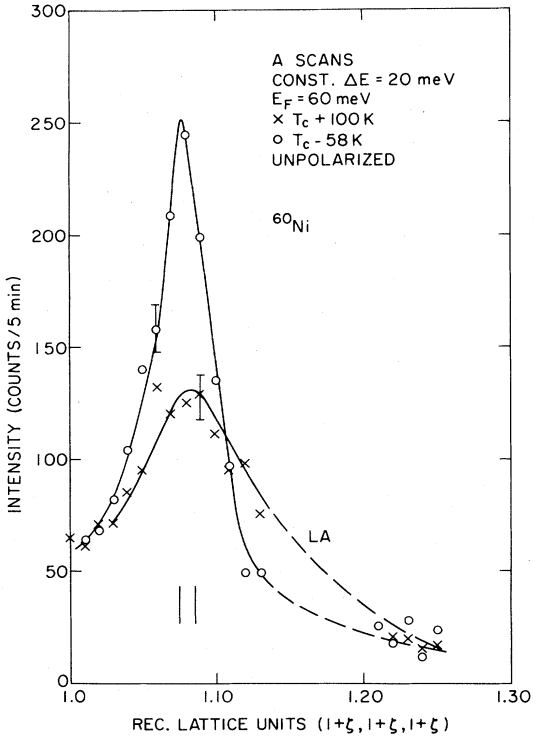

FIG. 3. The measurements drawn with circles show a spin-wave peak obtained at constant-energy transfer of 20 meV at T_C-58 K. The crosses show the magnetic ridge at T_C+100 K, also for $\Delta E=20$ meV (A scans in Fig. 2). The lines are guides to the eye.

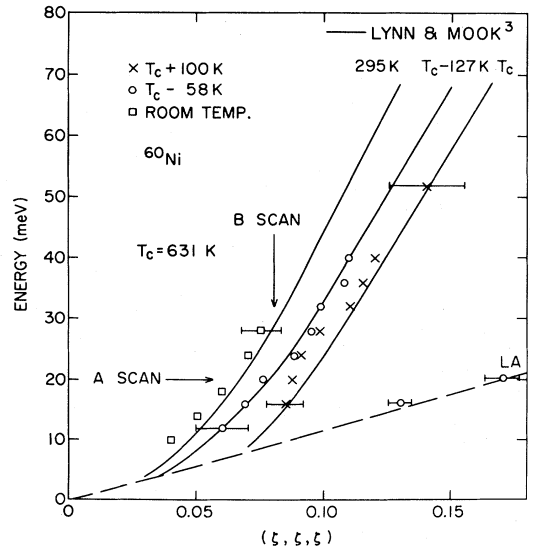

FIG. 2. The solid curves show the spin-wave dispersion curves as obtained by Lynn and Mook[3] for different temperatures $T\leq T_C$. The squares, circles, and crosses show the positions of the maxima of magnetic scattering obtained by us using constant-E scans with unpolarized neutrons. The longitudinal-acoustic phonon branch is labeled LA.

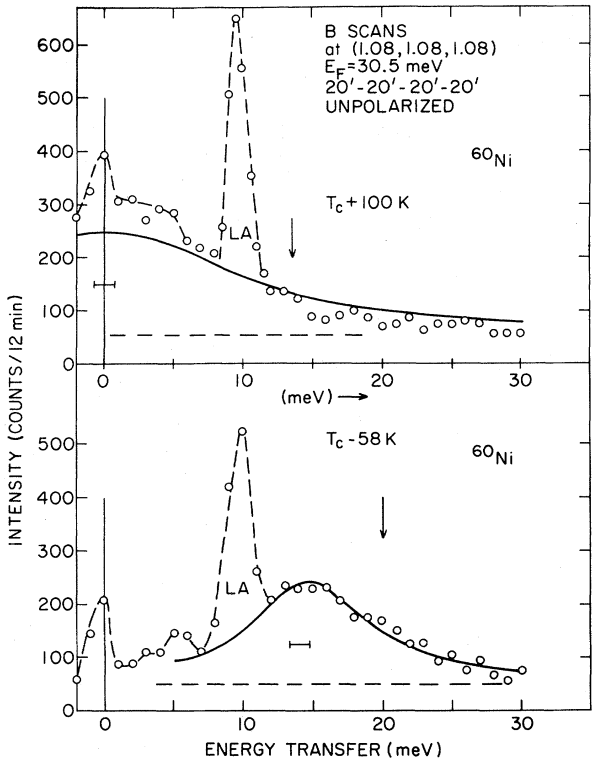

FIG. 4. The results of scans at constant momentum transfer at (1.08, 1.08, 1.08) for T_C-58 K and T_C+100 K (B scans in Fig. 2). The calculated cross sections for the magnetic scattering have been drawn with heavy lines as explained in the text. The arrow in the lower panel shows where the maximum intensity was expected to occur according to the dispersion curve in Fig. 2. The arrow in the upper inset points towards the expected spin-wave peak position. The horizontal bars show the energy resolution at zero energy transfer.

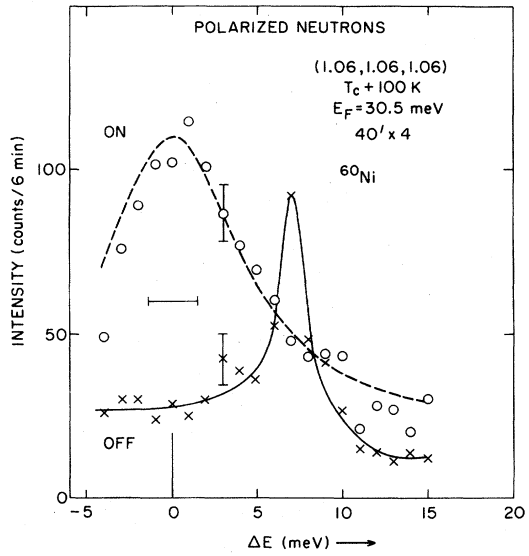

FIG. 5. The points along the dashed curve ("ON") were obtained in a constant-Q scan with polarized neutrons and spin-flip analysis for T_C+100 K. The crosses along the fully drawn curve ("OFF") were obtained with non-spin-flip analysis. The dashed line for ON data is the calculated cross section with parameters given in Ref. 1.

the maxima of intensity in our scans which, within the experimental error, are consistent with the dispersion curve of Lynn and Mook[3] for $T \geq T_C$. We also see that along the constant-Q scans at either (1.08,1.08,1.08) or (1.1,1.1,1.1) the intensities are decreasing monotonically as the energy increases yielding a Lorentzian line shape.

Constant-Q scans of the type illustrated in Figs. 4 and 5 give the spectral shape of the magnetic scattering above T_C. Integrating over energy for each q value results in a value of $S(Q)$ or $M^2(Q)$,

$$M^2(Q)=\int_{-\infty}^{\infty} S(Q,\omega)d\omega \ . \tag{2}$$

Using the conversion factor from the calibration curve, the integrated intensities may be converted into equivalent values first in b/atom and then into μ_B^2/atom. In Fig. 7, a plot of $M^2(Q)$ versus Q is given for data obtained via unpolarized and polarized neutrons at several temperatures above T_C. Smooth lines have drawn through the data points as a guide to the eye. These lines intersect the $q=0$ axis at values of $M^2(0)$ obtained from the static susceptibility. Also plotted in this figure is a straight line at the value $\mu_{\text{eff}}^2=2.58\mu_B^2$ which is the value of the paramagnetic response when there is no correlation between atomic spins. Even for temperatures up to T_C+150 K, the $M^2(Q)$ data surprisingly follow a Lorentzian-type curve which is normally characteristic of the critical scattering region close to T_C.

Minkiewicz *et al.*[1] have studied the linewidths Γ (half width at half maximum) of constant-Q scans on Ni at $T=T_C$ and found that the q dependence of the linewidths follows the predictions of dynamic scaling theory.[10] Setting $\Gamma=Aq^z$ they found that $A=330$ meV Å$^{-2.5}$ and $z=2.46\pm0.25$ whereas theory predicts $z=2.5$. We have plotted on the left-hand side of Fig. 8 our resolution-corrected data at T_C obtained with $E_F=14.7$ meV together with the data[12] from Ref. 1. The half-width values from our data fit in nicely with the data obtained by

TABLE I. Wave-vector (ΔQ) and energy (ΔE) resolutions at specific Q-values and energy transfers.

	$1+\zeta$	Q (Å^{-1})	E_i (meV)	E_F (meV)	Collimation	$\Delta\vec{Q}\|\|[111]$ (Å^{-1})	ΔQ_z (Å^{-1})	ΔE (meV)
Unpolarized	1.08	3.31	43.5	30.5	20'-20'-20'-20'	0.03	0.16	2.0
	1.13	3.45	104.0	60.0	40'-20'-20'-40'	0.20	0.22	10.1
Polarized	1.06	3.26	37.5	30.5	40'-40'-40'-40'	0.05	0.16	2.9

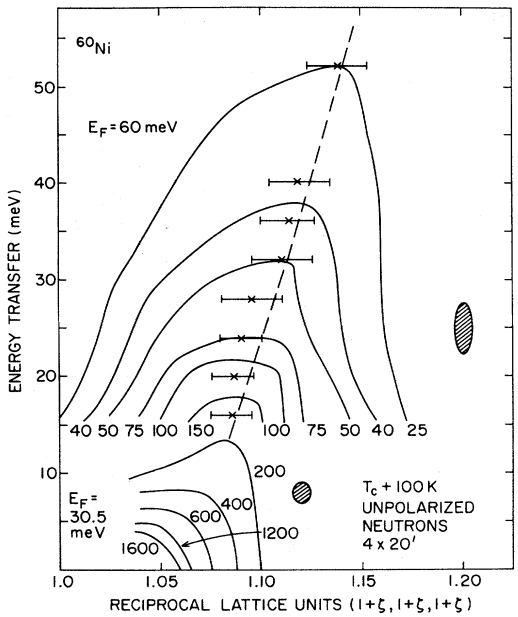

FIG. 6. A map of constant-intensity contours in (q,ω) space constructed from constant-Q scans at $E_F=30.5$ meV and constant-E scans at $E_F=60$ meV close to the (1,1,1) reciprocal-lattice point. The crosses show the approximate positions of the maxima of intensity in constant-E scans. The dashed line is the dispersion curve for the so-called persistent spin-wave mode taken from Ref. 3. The resolution ellipses for elastic scattering at 30.5 and 60 meV have also been drawn.

Minkiewicz *et al.*[1] On the right-hand side of Fig. 8 we have plotted the resolution-corrected energy widths at T_C+100 K for unpolarized and polarized neutrons. Comparing the right- and left-hand sides we see that the

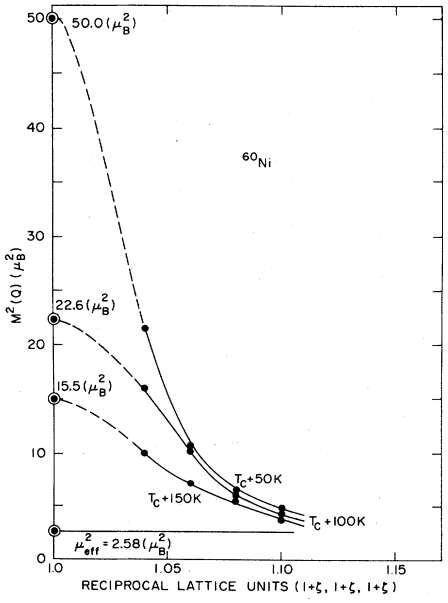

FIG. 7. The closed circles are averages of $M^2(Q)$ data obtained from polarized and unpolarized neutron measurements for a series of temperatures $T>T_C$. The curves drawn through the data points are guides to the eye.

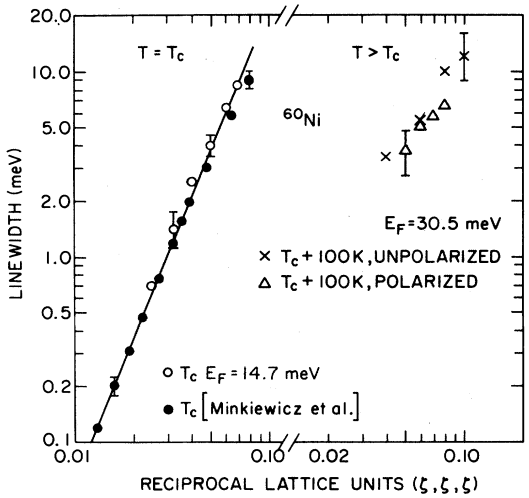

FIG. 8. The open circles on the left-hand side show experimental half widths at half maximum obtained by us at T_C for $E_F=14.7$ meV. The widths have been corrected for resolution effects. The closed circles are half widths from Ref. 1. The straight line (slope 2.5) is the best fit to these data. On the right-hand side are shown half widths obtained with polarized and unpolarized neutrons at T_C+100 K for $E_F=30.5$ meV.

widths are similar although the error bars on the right are larger due to the reduced intensities found at higher temperatures and larger q values. Using the half width of $\Gamma=5.5$ meV at $\zeta=0.06$ along with the expression for Γ used in the hydrodynamic region, $\Gamma=\Lambda q^2$, we obtain $\Lambda=160$ meV Å^2 which, within statical error, agrees with the value of $\Lambda=137$ meV Å^{-2} obtained by Minkiewicz *et al.*

Substituting Eq. (1) into Eq. (2) gives

$$M^2(Q)=M^2(0)\frac{\kappa_1^2}{\kappa_1^2+q^2}\,. \tag{3}$$

Equation (3) can now be compared with the energy-integrated constant-Q scans illustrated in Fig. 7. In Fig. 9, we compare the $M^2(Q)$ data at T_C+100 K with Eq. (3) using the value $M^2(0)=22.6\mu_B^2$ obtained from the static susceptibility and the value $\kappa_1=0.174$ Å^{-1} which has been scaled from the relation[10]

$$\kappa_1=\kappa_\infty\left[\frac{T-T_C}{T_C}\right]^\nu \tag{4}$$

with $\kappa_\infty=0.635$ Å^{-1} and $\nu=0.7$. We see that the Lorentzian curve obtained from Eq. (2) along with the value of κ_1 scaled from values in the critical region fits the $M^2(Q)$ data quite well.

A second comparison is seen in Fig. 10 where now the experimental $M^2(Q)$ data obtained by Brown *et al.*[6] using polarized neutrons around the (0,0,0) reciprocal lattice point at T_C+68 K have been plotted. The dashed curve is a Lorentzian determined, as above, from Eqs. (2) and (4) at T_C+50 K. Included in this figure are our own $M^2(Q)$ data obtained at T_C+50 K. There is an agreement between the two sets of measurements at moderate q values,

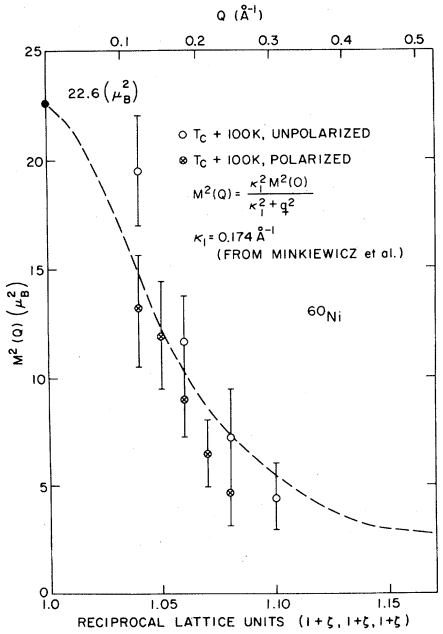

FIG. 9. The open circles show integrated magnetic intensities $M^2(Q)$ for the unpolarized neutron case at $T_C + 100$ K. ⊗ show similar integrated intensities obtained with polarized neutrons. The dashed curve is a Lorentzian for which $q=0$ goes through the value $M^2(0)=22.6\mu_B^2$ as obtained from the static susceptibility at this temperature.

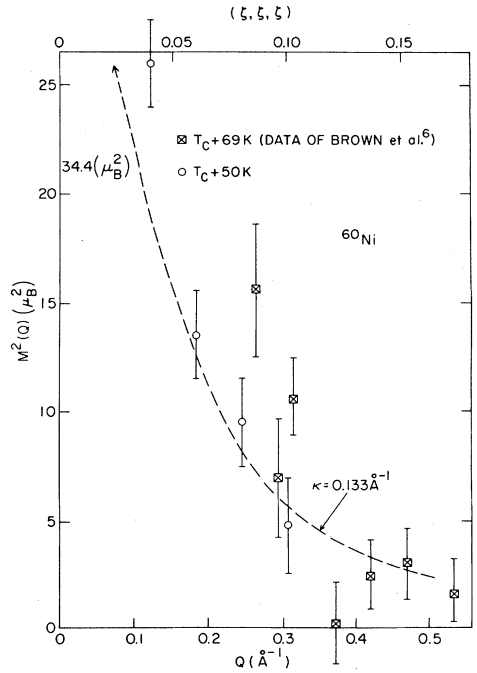

FIG. 10. The ⊠ show data of Brown *et al.*[6] for $M^2(Q)$ at $T_C + 68$ K obtained close to (0,0,0). The dashed curve is a Lorentzian going through $M^2(0)=34.4\mu_B^2$ with correlation length $1/\kappa_1=7.5$ Å. The open circles show our data obtained with unpolarized neutrons close to the (1,1,1) reciprocal-lattice point at $T_C + 50$ K.

but for smaller q values the data of Brown *et al.*[6] are considerably higher. The reason for this difference is not clear. However, the high neutron energies used by Brown *et al.*[6] make experiments at small angles very difficult. The background of multiple scattered neutrons tends to increase with neutron energy giving a polarization-dependent background. Once again, the Lorentzian form of $M^2(Q)$ fits the data reasonably well within the statistical error.

IV. DISCUSSION

The use of both polarized and unpolarized neutron scattering has allowed us to accurately investigate the paramagnetic scattering in ^{60}Ni. In constant-energy scans we observed a ridge of magnetic scattering which is very similar to the constant-energy peaks originally reported by Mook *et al.*[2] However, in constant-Q scans which covered energy transfers up to 50 meV, a broad Lorentzian distribution centered at zero energy transfer was observed with no additional enhancements occurring at finite energy transfer. These scans ranged in q from 0.06 to 0.4 Å^{-1} and covered a range of q in which Lynn and Mook[3] reported observing constant-energy spin waves beyond 35 meV ($q>0.35$ Å^{-1}) for temperatures up to $2T_C$.

The criterion used by Lynn and Mook[3] to determine whether the constant-energy peaks were propagating spin waves was $\Delta E/E<1$. Here E corresponds to the energy of the peak while ΔE is the energy width. Lynn and Mook[3] obtained this ratio by a conversion from $\Delta q/q$ using the spin-wave dispersion relation above T_C as shown in Fig. 2. It is obvious that such a conversion is not justified as can be seen from our contour map in Fig. 6.

We can demonstrate that the data of Lynn and Mook[3] are consistent with our conclusion that the spin-wave-like ridge constitutes a minor weight of the paramagnetic scattering. In our measurements we have confirmed that the observed integrated spin-wave intensities at different temperatures below T_C behave according to Eq. (A2) (see Appendix). In Ref. 3, Lynn and Mook present a graph showing the integrated intensity of spin wave scattering as a function of energy and temperature. Their curves for temperatures above T_C indicate, however, that their scattered intensity observed in constant-E scans are much smaller than that predicted for an "ideal" spin-wave intensity above T_C as can be calculated from Eq. (A2). When we look at their curve for 775 K, at the point $\Delta E=30$ meV [$q=0.33$ Å^{-1} or $\vec{q}\approx(1.1,1.1,1.1)$], we find that the observed spin-wave intensity is only 3.5% of what Eq. (A2) predicts and is equivalent to an absolute value of $0.17\mu_B^2$. This is very small when compared with our constant-Q scans where the total integrated intensity is equivalent to an absolute value of $3.7\mu_B^2$ at this momentum transfer. The minor spectral weight "persistent spin waves" is clear when it is put on the proper scale with the data in absolute units.

Cowley[13] first suggested to us that a simple paramagnet obeying a scattering function like Eq. (1) which is Lorentzian in both q and ω would show a peak in constant-energy scans. Our experiments clearly indicate

that this hypothesis by Cowley is correct. The constant-Q scans are clearly Lorentzian in energy while the energy-integrated intensity $M^2(Q)$ [see Eq. (3)] illustrates a Lorentzian behavior in q (Figs. 9 and 10). The peak position and FWHM of both Lynn and Mook[3] and our constant-energy measurements for energy transfers up to 50 meV can be explained quite well using the form of $S(Q,\omega)$ given in Eq. (1) with $\Gamma=\Lambda q^2$. Here Λ, as well as κ_1, has been scaled from the hydrodynamic region using values obtained by Minkiewicz *et al.*[1] However, we still had believed that for energy transfers beyond 50 meV, the magnetic scattering above T_C must be due to spin waves.

After the completion of these experiments and analysis on ^{60}Ni, Uemura *et al.*[14] made an interesting observation. All constant-energy data up to 80 meV obtained by Lynn and Mook,[3] in addition to the results of Brown *et al.*[6] and our constant-Q results, could be explained by Eq. (1) provided that near T_C, for $q>\kappa_1$, a change from $\Gamma=\Lambda q^2$ to $\Gamma=Aq^{2.5}$ is made. It was also demonstrated that Eq. (1), using the proper change over for Γ, can describe the paramagnetic scattering from localized systems such as EuO as well as an itinerant ferromagnet like Ni. It was then realized[15] that at $T=T_C$, the scattering function becomes a universal function

$$S(Q,\omega)\propto\frac{1}{A}\frac{q^{0.5}}{q^5+(\omega/A)^2}\ , \tag{5}$$

i.e., the cross section for all isotropic ferromagnets is identical at T_C provided the energy is scaled by A.

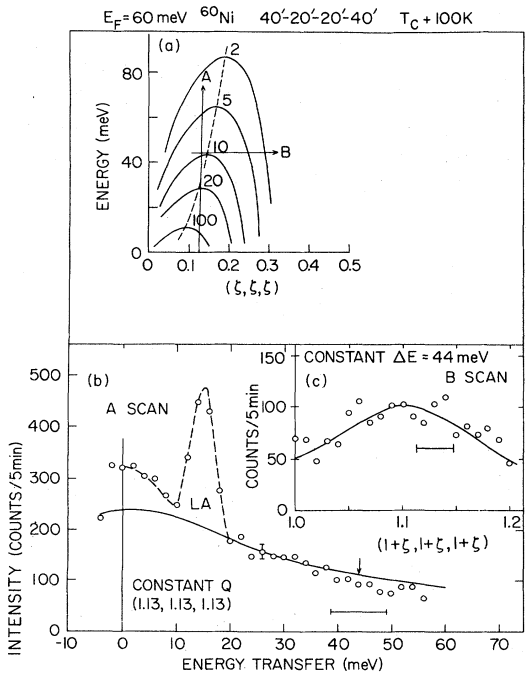

FIG. 11. (a) Demonstration of the peak in constant-E scan and the diffusive nature in constant-Q scans for $\zeta=1.13$. The solid line in (b) is calculated with $\Gamma=25$ meV with appropriate resolution convolution.

The idea of explaining the constant-E ridges by the double Lorentzian [Eq. (1)] had apparently occurred to many scientists during the past ten years when the persistent spin-wave pictures prevailed. In 1974, soon after the first results of Mook *et al.*[2] on Ni were published, Collins[16] made a revealing observation. He noticed that the constant-E ridges at small energies can be explained by Eq. (1), but did not pursue this further. Then Lynn and Mook stated in their Ni paper[3] that their calculation of the widths of the constant ridges using Eq. (1) is five times wider than observed. We did not understand their results, particularly after the reasonably successful model calculations by Uemura *et al.*[14] The reason for their failure became apparent when Lynn published very recently an addendum[17] (to his earlier Fe data) which included a model calculation using $\Gamma=\Lambda q^2$, $\Lambda=20$ meV Å^2; this Λ corresponds to $\Lambda(T)$ very near T_C. If one does not change over to $Aq^{2.5}$ a large error results.

After this study on Ni was completed, Wicksted, Böni, and Shirane[18] carried out similar but more definitive studies of paramagnetic scattering from Fe. They demonstrated that the detail shape of the constant-E scans are very sensitive to the secondary parameters of the scattering function. For example, an expected deviation from the strictly Lorentzian shape in ω drastically modifies the positions and shapes of the constant-E ridge, though the same deviation has only a minor effect on a constant-Q peak. We believe that essential characteristics of constant-E scans for Ni, as well as Fe, are now in accord with the paramagnetic scattering function we have used in this study.

Finally, let us examine the meaning of the changeover energy of 35 meV, above which Lynn and Mook[3] claimed propagating spin waves above T_C. We arrived at this value by converting $\Delta q/q$ to $\Delta E/E$ by utilizing the "dispersion curve." We have demonstrated convincingly that this conversion is not valid; the value 35 meV loses its meaning completely. Nevertheless, we show in Fig. 11 a constant-Q scan which is beyond this 35-meV cutoff. Again, no trace of the spin wave enhancement is seen at the arrow, where constant-E ridges indicated the spin wave.

Then we have to ask the question where do we find the essential differences between MnSi, Ni, and EuO. It is possible, though not proven yet, that an important deviation from Eq. (1) does take place at higher energies. Another line of thought is to assume that basic parameters, such as T_C, D, A, and κ_0, contain most of the pertinent information. Work is now in progress on a series of cubic ferromagnets (EuO, Pd_2MnSn, Fe_3Pt).

ACKNOWLEDGMENTS

We would like to thank R. A. Cowley, Y. Ishikawa, and Y. J. Uemura for many helpful discussions. Work at Brookhaven supported by the Division of Materials Sciences, U.S. Department of Energy under Contract No. DE-AC02-76CH00016.

APPENDIX: ABSOLUTE CROSS-SECTION MEASUREMENTS

A calibration technique will now be described which allows all paramagnetic scattering measurements to be put onto an absolute intensity scale in μ_B^2. Ziebeck and Brown[19] have successfully utilized the integrated intensity in powder Bragg peaks for such normalization purposes. However, when the sample is a single crystal it is better to use coherent phonon and magnon peaks for the normalization. The absolute cross sections are easily calculated from known formulas.

Chesser and Axe[20] have demonstrated that the integrated intensity I in an inelastic peak for constant-Q scan can be written as a product of two factors, one depending only on the specimen and the other, only depending on the instrument. If all the measurements are made as a function of a constant monitor count with fixed final neutron energy E_F then the dependence on K_I drops out and the instrumental factor is a constant for all scans.

Based on the known differential scattering cross sections for phonon and magnon scattering[21] we have

$$\left[\frac{d\sigma}{d\Omega}\right]_{\text{phonon}} = B\frac{\bar{b}^2 Q^2 \cos^2\beta}{M\omega}\langle n+1\rangle \exp(-2W)N \ . \quad \text{(A1)}$$

In order to make a convenient formula we have drawn together all factors relating to units in the parameter B which has the value 2.09 b/atom. The rest of the parameters may then be considered as numbers where $\bar{b}^2$ is the nuclear coherent scattering length in b, $\vec{Q}$ is the scattering vector measured in Å^{-1}, β is the angle between the phonon polarization vector and $\vec{Q}$, M is the atomic weight in amu, ω is the energy transferred to the sample in meV, $\langle n+1\rangle$ is the Bose occupation number, $\exp(-2W)$ is the Debye-Waller factor and N is the number of scattering atoms in the sample.

A similar expression for magnon scattering is

$$\left[\frac{d\sigma}{d\Omega}\right]_{\text{magnon}} = \tfrac{1}{2}\gamma_0^2 S f^2(\vec{Q})(1+Q_z^2) \times \langle n+1\rangle \exp(-2W)N \ , \quad \text{(A2)}$$

where γ_0^2 is 0.292 b, S is the atomic spin, and $f(Q)$ is the magnetic form factor. For a cubic crystal without a magnetic field the average of $1+Q_z^2$ over many domains is $\frac{4}{3}$. The spectrometer normalization then consists of using the equations (A1) and (A2) above to calculate the pertinent scattering cross sections in b/atom and plotting the measured integrated neutron counts versus the calculated values. We may then draw a line of best fit through the points.

This normalization procedure has been successfully applied to several monatomic metals and compounds. An example of such a calibration curve is shown in Fig. 1 in the main text. We have avoided using the incoherent scattering for normalization purposes since this scattering is normally weak in ^{60}Ni. In addition this requires that the crystal be a true single crystal since small misaligned crystallites in the sample will contribute to the incoherent scattering, but not, for example, to phonon or magnetic scattering.

With the normalized constant for the spectrometer at hand it is possible to extend the scaling procedure to the paramagnetic region of magnetic crystals. For the simple case of paramagnetic scattering from a system of N spins without spin correlations we have

$$\left[\frac{d\sigma}{d\Omega}\right]_{\text{para}} = \tfrac{1}{6}\gamma_0^2 f^2(Q)\exp(-2W)4S(S+1)N \ . \quad \text{(A3)}$$

An effective magnetic moment per atom, μ_{eff}^2, may be defined as

$$\mu_{\text{eff}}^2 = 4S(S+1) \ .$$

In the general case of scattering from itinerant systems the exact formula for the paramagnetic scattering is not known. However, the energy-integrated intensity of the magnetic scattering can be measured experimentally and the equivalent value of $(d\sigma/d\Omega)_{\text{expt para}}$ (in barns) can be calculated by using the normalization constant. Further, by the analog of Eq. (A3) we may derive the experimental wave-vector-dependent magnetic response, $M^2(Q)$. The value of $M^2(Q)$ will then be in μ_B^2/atom. It should also be noted that the magnetic scattering $S(Q,\omega)$ can be put into units of μ_B^2 and the cross section into millibarns per unit energy using this same calibration procedure.

*Permanent address: Institute for Energy Technology, 2007 Kjeller, Norway.

[1]V. J. Minkiewicz, M. F. Collins, R. Nathans, and G. Shirane, Phys. Rev. **182**, 624 (1969).

[2]H. A. Mook, J. W. Lynn, and R. M. Nicklow, Phys. Rev. Lett. **30**, 556 (1973).

[3]J. W. Lynn and H. A. Mook, Phys. Rev. B **23**, 198 (1981).

[4]J. W. Lynn, Phys. Rev. B **16**, 2624 (1975).

[5]V. Korenman, J. Murray, and R. E. Prange, Phys. Rev. B **16**, 4032 (1977); J. B. Sokoloff, J. Phys. F **5**, 1946 (1975); H. Capellmann, Z. Phys. B **34**, 29 (1979); M. V. You, V. Heine, A. J. Holden, and P. J. Lin-Chung, Phys. Rev. Lett. **44**, 1282 (1980).

[6]P. J. Brown, H. Capellmann, J. Deportes, D. Givord, and K. R. A. Ziebeck, J. Magn. Magn. Mater. **31-34**, 295 (1983).

[7]P. J. Brown, H. Capellmann, J. Deportes, D. Givord, and K. R. A. Ziebeck, J. Magn. Magn. Mater. **30**, 243 (1982).

[8]D. M. Edwards, J. Magn. Magn. Mater. **36**, 213 (1983).

[9]O. Steinsvoll, C. F. Majkrzak, G. Shirane, and J. Wicksted, Phys. Rev. Lett. **51**, 300 (1983).

[10]A comprehensive review of the scattering formulas and scaling relations for the Heisenberg ferromagnet EuO is given by O. W. Dietrich, J. Als-Nielsen, and L. Passell, Phys. Rev. B **14**, 4923 (1976).

[11]J. Skalyo, Jr. and N. A. Lurie, Nucl. Instrum. Methods **112**, 571 (1973).

[12]The extent of the linewidth data obtained from Ref. 1 was inadvertently misquoted in our previous publication (Ref. 9).

[13]R. A. Cowley (private communication).
[14]Y. J. Uemura, G. Shirane, O. Steinsvoll, and J. Wicksted, Phys. Rev. Lett. **51**, 2322 (1983).
[15]G. Shirane, O. Steinsvoll, Y. J. Uemura, and J. Wicksted, J. Appl. Phys. **55**, 1887 (1984).
[16]M. Collins (unpublished).
[17]J. W. Lynn, Phys. Rev. B **28**, 6550 (1983).
[18]J. Wicksted, P. Böni, and G. Shirane, Phys. Rev. B (to be published).
[19]K. R. A. Ziebeck and P. J. Brown, J. Phys. F **10**, 2015 (1980).
[20]N. J. Chesser and J. D. Axe, Acta Crystallogr. Sect. A **29**, 160 (1973).
[21]G. L. Squires, in *Introduction to the Theory of Thermal Neutron Scattering* (Cambridge University Press, Cambridge, England, 1978).